ISSN 0027-1349, Moscow University Physics Bulletin, 2010, Vol. 65, No. 6, pp. 477–482. © Allerton Press, Inc., 2010.
Original Russian Text © A.M. Lerer, G.P. Sinyavsky, 2010, published in Vestnik Moskovskogo Universiteta. Fizika, 2010, No. 6, pp. 48–53.

Diffraction of an Electromagnetic Wave on the Finite Lattice of Carbon Nanotubes–Vibrators Located at Dielectric Interfaces

A. M. Lerer and G. P. Sinyavsky

Southern Federal University, ul, Zorge 5, Rostov-on-Don, 344090 Russia
e-mail: lerer@sfedu.ru

Received May 5, 2010; in final form, July 24, 2010

Abstract—A solution of the boundary problem on electromagnetic wave diffraction on a lattice of carbon nanotubes–vibrators is reduced to the solution of a set of integrodifferential equations, whose kernels are represented as a Fourier integral. Such representation of kernels makes it possible to easily overcome solution problems related to their singularities and reduce the computation time by one order of magnitude. Integrodifferential equations are solved using the Galerkin method with a Chebyshev basis. The effect of a substrate on amplitude–frequency characteristics and the scattering pattern of carbon nanotube antennas is studied. Both the resonance frequency and the amplitude of a scattered field are shown to increase in the case of approaching nanovibrators. The amplitude dependence on the number of vibrators is nonlinear.

Keywords: carbon nanotubes, nanotubes–vibrators, millimeter wavelength range antennas, integral equations, Galerkin method, resonance, scattering pattern.

DOI: 10.3103/S0027134910060093

INTRODUCTION

The possibility of using carbon nanotubes (CNT) as antennas of centimeter and millimeter wavelength ranges is being currently considered. Such antennas can be used for interconnecting nanoelectronic circuits and macroscopic devices. The authors of [1–7] note that their electric lengths that are larger as compared to metallic vibrators. Owing to this, the resonances of input resistance are observed in the millimeter range in 20–50 μm-long nanotubes–vibrators. The conductance of nanotubes is higher than that in the majority of known conductors of comparable sizes.

Nanoantennas of an optical wavelength range made of multiwall carbon nanotubes (MCNT) were experimentally studied in [8]. MCNTs are 80–100 nm in diameter, which is two times larger as compared to CNT diameters. It has been revealed that the characteristics of MCNT antennas are closer to those of antennas made of metallic nanowires than to CNT antennas. This is explained by the fact that the plasma frequency of MCNTs is substantially higher as compared to CNTs.

The majority of theoretical studies analyze an idealized model, namely a CNT in a vacuum, and only a CNT in [9] rests on a dielectric substrate. In accordance with the standard technique of CNT growing, they are positioned perpendicular to a substrate.

The aim of the present study is to investigate the diffraction characteristics of an antenna consisting of CNT-vibrators arbitrarily positioned perpendicular to a substrate. The method of solving the thus-formulated problem is similar to that described in [9] where the solution of a boundary problem on the excitation of a vibrator (a carbon nanotube) is reduced to the solution of paired integral equations (PIEs) with respect to the Fourier transform for the vibrator current density. When solving PIEs, the peculiarity of the kernel of integrodifferential equations (IDE) for the vibrator current density lies in the slow convergence of integrals in the spectral space. It is easier to improve convergence of integrals than to perform IDE regularization.

Consider a CNT entirely located in a dielectric with the permittivity ε_1 perpendicular to a dielectric substrate ε_2, $\mu_1 = \mu_2 = 1$ (see the insert in Fig. 1). Let us introduce a Cartesian system of coordinates where the X and Y axes are parallel to a substrate and perpendicular to a CNT, the Z-axis is directed along the vibrator perpendicular to a substrate, and the origin is on a substrate. The length of the CNT is L and its radius is a.

The quantum-mechanical properties of a carbon nanotube in the modes, as those in the majority of theoretical studies, are described with the use of a macroscopic parameter, namely, surface impedance. Assume that the following boundary condition holds for the vibrator surface

$$E_z = \rho_s j, \tag{1}$$

where E_z, j are the longitudinal components of the electric field intensity, ρ_s is the surface resistance of the

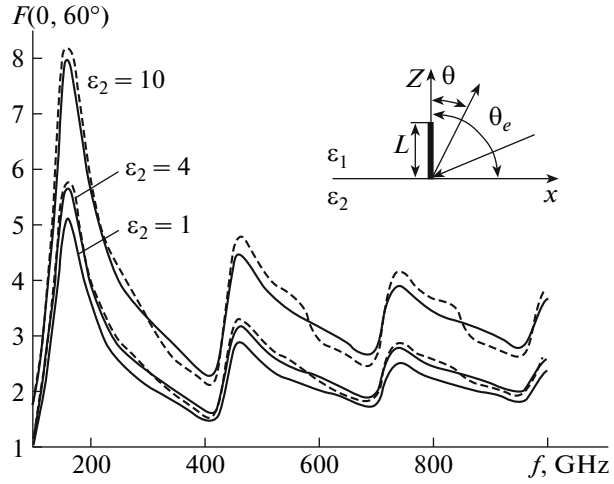

Fig. 1. The amplitude of the field in the far zone of a single nanovibrator as a function of frequency. The incidence and observation angles are 60°, $\varepsilon_2 = 1, 4, 10$. Solid curves: the second term in GF (14) is truncated; dashed lines: exact GF.

nanotube [5] equal to $\rho_s = i\dfrac{\pi^2 a\hbar(\omega - i\nu)}{2e^2 v_F}$, where v_F is the Fermi velocity (for a CNT $v_F = 9.71 \times 10^5$ m/s), ω is the cyclic frequency. ν is the relaxation frequency (for a CNT, $\nu = 3.33 \times 10^{11}$ Hz), e is the electron charge, c is the light velocity in vacuum, and $\hbar$ is the Plank constant.

1. A SINGLE CNT-VIBRATOR

We first consider a single CNT–vibrator. As usual, we assume that there is only a longitudinal current component on the vibrator that depends only on z and that it meets boundary condition (1). Thus, we obtain the integrodifferential equation

$$\frac{1}{i\omega\varepsilon_1\varepsilon_0}\left(\frac{d^2}{dz^2} + k_1^2\right)\int_0^L j(z')g_e(z, z')dz' + E_z^e(z) = \rho_s j(z), \text{ at } z \in [0, L], \tag{2}$$

where $E_z^e(z)$ is the external field, k_1 is the wave number in the upper dielectric, and the IDE kernel will be determined below.

We solve IDE (2) using the Galerkin method. The weighted Chebyshev polynomials of the second kind will be used as basis functions [9].

$$V_n(z) = \frac{i^n}{\pi(n+1)}\sqrt{1 - z^2/l^2}\,U_n\left(\frac{z}{l}\right), \quad n = 0, 1, 2\ldots$$

The solution of IDE (2) yields a set of linear algebraic equations (SLAE) with respect to the unknown X_n.

$$\sum_{n=0}^{\infty} X_n\left[A_{mn} - \rho_s\int_0^L V_m^*(z)V_n(z)dz\right] = -\int_0^L E_z^e(z)V_m^*(z)dz, \quad m = 0, 1\ldots$$

where

$$A_{mn} = \frac{1}{i\omega\varepsilon_1\varepsilon_0}\int_0^L dz V_m^*(z)\left(\frac{d^2}{dz^2} + k_1^2\right) \times \int_0^L V_n(z')g_e(z, z')dz'. \tag{3}$$

The main problem in estimating matrix elements (ME) A_{mn} is associated with the logarithmic peculiarity of the IDE kernel $g_e(z, z')$. The method for calculating ME for an ideally conducting vibrator is described in [10]. There is another possible approach to calculating matrix elements, namely, the use of an integral representation (IR) of the kernel [9]

$$g_e(z, z') = \int_0^{\infty}\tilde{g}_e(\rho, z, z')d\rho.$$

Then

$$A_{mn} = \frac{1}{i\omega\varepsilon_1\varepsilon_0}\int_0^{\infty}\tilde{A}_{mn}(\rho)d\rho, \tag{4}$$

and IR kernels should be such that the integrals

$$A_{mn}(\rho) = \int_0^L dz V_m^*(z)\left(\frac{d^2}{dz^2} + k_1^2\right)\int_0^L V_n(z')\tilde{g}_e(\rho, z, z')dz'$$

were taken analytically. The peculiarity of an IDE kernel lies in the slow convergence of the integral over ρ in Eq. (4). It is easier to improve the integral convergence and numerically integrate Eq. (4) than to perform double integration of the functions with the singularity (3).

We determine an IDE kernel

$$g_e(z, z') = \frac{a}{2\pi}\int_0^{2\pi}d\varphi\int_0^{2\pi}g(x, x', y, y', z, z')d\varphi'. \tag{5}$$

It is assumed in Eq. (5) that the observation and source points are on the vibrator surface

$$x = a\cos\varphi, \quad y = a\sin\varphi, \quad x' = a\cos\varphi', \quad y' = a\sin\varphi'. \tag{6}$$

The function $g(x, x', y, y', z, z')$ is the Green function (GF) for the vector potential in case of a current perpendicular to the substrate. At $z \geq 0$ and $z' \geq 0$, the GF has the form [10]

$$g(x, x', y, y', z, z') = \frac{1}{8\pi^2}\int_{-\infty}^{\infty}\int_{-\infty}^{\infty}[e^{-\gamma_1|z-z'|} + Q(\rho)e^{-\gamma_1(z+z')}]\frac{1}{\gamma_1}e^{i\alpha\bar{x}+i\beta\bar{y}}d\alpha d\beta, \quad (7)$$

where $\bar{x} = x - x'$, $\bar{y} = y - y'$, $Q = \frac{\gamma_1 - \gamma_2 t}{\gamma_1 + \gamma_2 t}$, $t = \frac{\varepsilon_1}{\varepsilon_2}$, $\gamma_{1,2} = \sqrt{\rho^2 - k_{1,2}^2}$, $\rho = \sqrt{\alpha^2 + \beta^2}$, and k_2 is the wave number in a substrate.

The first term in Eq. (7) in the GF of a free space

$$g_0(x, x', y, y', z, z') = \frac{1}{8\pi^2}\int_{-\infty}^{\infty}\int_{-\infty}^{\infty}e^{-\gamma_1|z-z'|}\frac{1}{\gamma_1}e^{i\alpha\bar{x}+i\beta\bar{y}}d\alpha d\beta \quad (8)$$

which is known to be expressed analytically as

$$g_0(x, x', y, y', z, z') = \frac{e^{-ik_1R}}{4\pi R}, \quad (9)$$

$$R = \sqrt{(x-x')^2 + (y-y')^2 + (z-z')^2}.$$

The Green function g_0 can be also represented as the Fourier integral

$$g_0(x, x', y, y', z, z') = \frac{1}{4\pi^2}\int_{-\infty}^{\infty}K_0(\gamma_1 r)e^{i\rho(z-z')}d\rho = \frac{1}{2\pi^2}\int_{-\infty}^{\infty}K_0(\gamma_1 r)\cos(\rho(z-z'))d\rho, \quad (10)$$

where $r = \sqrt{(x-x')^2 + (y-y')^2}$, K_0 is a modified Bessel function of the second kind. An advantage of the integral representation of GF (10) over IR (8) is due to the fact that it makes it possible to take integrals (4) analytically.

Substituting Eq. (10) into Eq. (5) and taking Eq. (6) into account, we get

$$g_{e,0}(z, z') = \frac{a}{2\pi}\int_{-}^{\infty}I_0(\gamma_1 a)K_0(\gamma_1 a)e^{i\rho(z-z')}d\rho. \quad (11)$$

The second term in Eq. (7)

$$g_1(x, x', y, y', z, z') = \frac{1}{8\pi^2}\int_{-\infty}^{\infty}\int_{-\infty}^{\infty}Q(\rho)e^{-\gamma_1(z+z')}\frac{1}{\gamma_1}e^{i\alpha\bar{x}+i\beta\bar{y}}d\alpha d\beta \quad (12)$$

takes the substrate effect into account. At $\varepsilon_1 = \varepsilon_2$, $g_1 = 0$.

We substitute Eq. (12) into Eq. (5), taking Eq. (6) into account, and change the variables $\alpha = \rho\cos\vartheta$ and $\beta = \rho\sin\vartheta$. As a result we get

$$g_{e,1}(z, z') = \frac{a}{2}\int_0^{\infty}\rho Q(\rho)\frac{e^{-\gamma_1(z+z')}}{\gamma_1}J_0^2(\rho a)d\rho, \quad (13)$$

where $J_0(\rho a)$ is a Bessel function.

Thus, we get integral representations (11), (13) of the IDE kernel

$$g_e(z, z') = g_{e,0}(z, z') + g_{e,1}(z, z'). \quad (14)$$

Further transformations of ME, improvement of integral convergence included, are given in [9].

A method for calculating the field in the far zone is described in the Appendix. The external field is assumed to be the plane wave

$$E^e = E_0\exp[i(k_x x + k_y y + k_z z)],$$

where $k_x = k\cos\varphi_e\sin\theta_e$, $k_y = k\sin\varphi_e\sin\theta_e$, and $k_z = k\cos\theta_e$.

The electric field intensity in the far zone has only one component

$$E_\theta(r, \varphi, \theta) = F(\varphi, \theta)E_0\frac{\exp(-ikr)}{4\pi r/a}.$$

Let us analyze the internal convergence of the solution. The number of basis functions M naturally increases with an increase in the electric length of a CNT and in ε_1, but almost does not depend on the number of CNTs and ε_2. For $F(\varphi, \theta)$ to be calculated with an internal convergence error of less than 1% at $f = 250$ GHz (a half-length of a plasma wave propagating along a CNT lays on the vibrator), it is sufficient to assume that $M = 5$, with that at $f = 1000$ GHz (eight half-waves) being $M = 20$.

The frequency dependence of a scattered field is of the resonance type. Figure 1 shows the calculations at the incidence angle $\theta_e = 60°$. The sizes of CNTs here and hereinafter are $L = 20$ μm and $a = 0.02712$ μm. The resonance frequency of a CNT vibrator is nearly 50 times lower than that of an ideally conducting vibrator of the same size. The resonance frequency practically does not depend on the substrate permittivity ε_2. Naturally, only the scattered wave frequency varies. If we neglect the second term in Eq. (14), which takes the substrate into account, the results of the IDE solution change only negligibly. This is related to the fact that the current at the CNT ends is low. Thus, the substrate slightly affects the current distribution. This substantially quickens calculations. Both terms in GF (7) must be taken into account when calculating a scattered field.

The shape of the scattering pattern (SP) of a nanovibrator on a substrate (Fig.1) weakly depends on frequency, substrate permittivity at $\varepsilon_2 > 2$, and the incidence angle. Even for the second resonance frequency, a SP has only one directional lobe. This is explained by the fact that resonances in the amplitude–frequency characteristics of a scattered field and the current distribution on a vibrator are determined by the ratio of the vibrator length to the length of a plasma wave in a CNT. The SP shape, in particular, the number of lobes, mainly depends on the ratio of the vibrator length to the wavelength in a free space λ. For a CNT vibrator, $L/\lambda = 0.1$ even at $f = 1500$ GHz. In the case

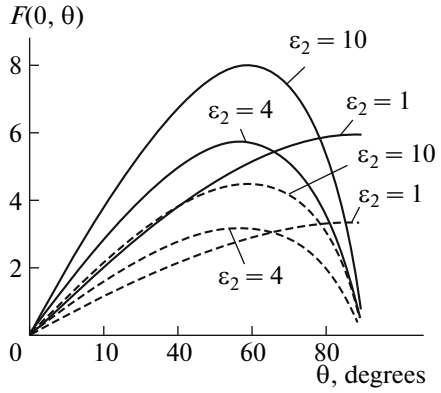

Fig. 2. The scattering pattern of a single CNT vibrator: $f =$ 162 GHz is the first resonance (solid curves), $f = 462$ GHz is the second resonance (dashed curves). $\theta_e = 60°$.

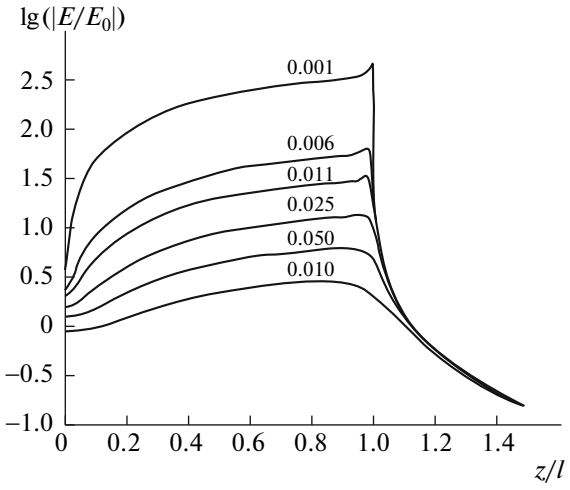

Fig. 3. The normalized intensity of the magnetic field near a nanovibrator. The figures near the curves mark the distance from a nanotube normalized to $l = L/2$.

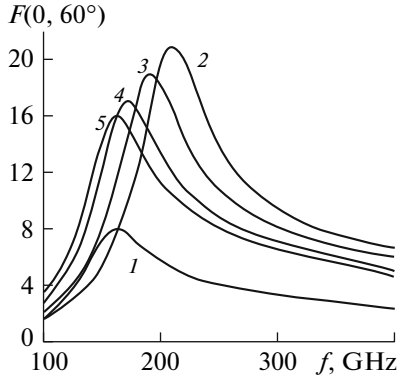

Fig. 4. The field in the far zone as a function of frequency for CNT. (Curve *1*) for one CNT; (Curves 2–5) for two CNTs: (curve *2*) the distance between CNTs is 0.02 μm, (curve *3*) 0.2 μm, (curve *4*) 2 μm, and (curve *5*) 50 μm.

of a single vibrator the SP does not depend on the angle φ.

Figure 3 shows the results of calculations of the field in the near zone of a CNT without a substrate. The coordinate origin is in the CNT center, Owing to symmetry, the field is shown only at $z > 0$. Near a CNT the field is 2–3 times higher than the external field. The field intensity sharply decreases when moving off a CNT.

2. A LATTICE OF CNT VIBRATORS

Let us consider now the diffraction of a system consisting of several CNT vibrators. In this case, it is also not difficult both to write a set of IDEs and derive their solutions using the Galerkin method. The matrix elements in a SLAE that describe the interaction of vibrators also have the form of Eq. (3), except that the points of source z' and observation z are located at different CNTs. The GF in this case does not have any singularity. Thus, it is natural to use a GF in the form of Eq. (9) and to take the integrals in Eq. (3) numerically by the quadratures of the maximal accuracy as it was done in [10]. However, the distance between CNTs can be much smaller than their length. In this case, the order of quadratires and the counting time sharply increase. Thus, in the present study we isolated the static part in Eq. (9) and used an integral representation

$$\frac{1}{R} = \frac{1}{\pi}\int_{-\infty}^{\infty} K_0(\gamma r) e^{i\gamma(z-z')} d\gamma,$$

$$g_0(x, x', y, y', z, z') = g_{01}(x, x', y, y', z, z') + g_{02}(x, x', y, y', z, z')$$

$$= \frac{1}{4\pi}\left[\frac{e^{-ik_1 R} - 1}{R} + \frac{1}{\pi}\int_{-\infty}^{\infty} K_0(\gamma r) e^{i\gamma(z-z')} d\gamma\right].$$

The integrals of the form of Eq. (3) with the GF g_{01} can now be easily found numerically at any R. The matrix elements with g_{02} are now expressed through a Fourier integral. Transformations of these matrix elements, improvement of integral convergence included, are analogous to those given in [9]. Since they are frequency-independent, it is sufficient to calculate them only once. This method of calculations shortens the counting time at small distances between nanovibrators by dozens of times.

Figures 4 and 5 show the frequency characteristics of CNT systems. The angles of incidence are $\varphi_e = \varphi = 0$, $\theta_e = \theta = 60°$, and the substrate is $\varepsilon_2 = 10$. The CNTs are positioned on the X axis and along the circle. For the sake of comparison, Fig. 4 also demonstrates the characteristics of one nanovibrator. The resonance frequencies f_n of the system of ordinary vibrators are the same as the resonance frequencies of the single vibrator

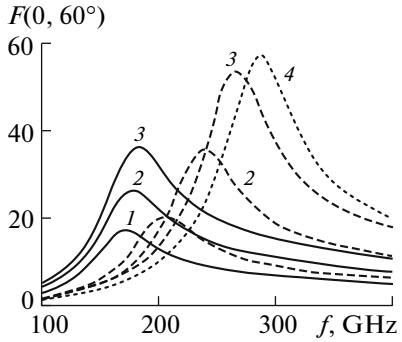

Fig. 5. The field in the far zone as a function of frequency for different numbers of CNTs. Systems of nanotubes: linear (curves *1*–*3*) and circular (CNTs are positioned in a circle) (curve *4*). Curve *1*, *2* CNTs, curve *2*, *3* CNTs, curve *3*, *4* CNTs. Solid curves, the distance between CNTs is 2 μm; dashed curves, 0.03 μm. The circle radius is 0.01 μm.

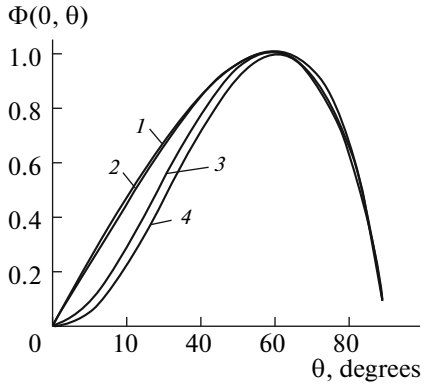

Fig. 6. The normalized scattering pattern in the *E*-plane. $\theta_e = 60°$ (curves *1*–*3*), $\theta_e = 80°$ (curve *4*). The distances between CNTs: 20 μm (curve *1*), 100 μm (curve *2*), and 300 μm (curves *3*, *4*).

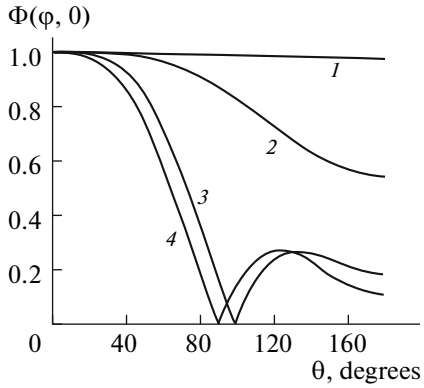

Fig. 7. the normalized scattering pattern in the *H*-plane. For curve labels see Fig. 6.

$$f_n = \frac{cn}{2(L + \Delta L)}, \tag{15}$$

where the effective vibrator length $L + \Delta L$ depends on the a/L ratio and the frequency. For a CNT, it is necessary to replace the light velocity in a vacuum in Eq. (15) with v, namely, the velocity of surface plasma waves in the CNT. This velocity for a single CNT and a system of connected CNTs is different owing to an interaction between CNTs. Since the waves are surface waves, the resonance frequency of a CNT system at the distances between CNTs on the order of 10 μm is the same as that in a single CNT. The value of v changes when CNTs approach one another and both the resonance frequency and the scattered field amplitude increase. In this case, the dependence of the amplitude on the number of nanovibrators is nonlinear.

Figures 6 and 7 show the results of the calculations of scattering patterns normalized to the maximal value. Four CNTs are positioned on the X-axis, the substrate in $\varepsilon_2 = 10$, $f = 250$ gHz, and $\varphi_e = 0$. The SP in the *E*-plane weakly depends on the number of CNTs and the distances between them. For a lattice of CNT vibrators to have directivity on the H-plane, the distance between the CNTs, as that between ordinary vibrators, should be on the order of one-fourth of the wavelength in a vacuum (Fig. 7). Thus, it is impossible to construct a directional nanosize antenna array from CNTs.

CONCLUSIONS

The solution of the boundary problem on the diffraction of an electromagnetic wave on a lattice from carbon nanotubes–vibrators is reduced to the solution of a set of integrodifferential equations, the kernels of which are represented as a Fourier integral. Using the Galerkin method with the Chebyshev basis, the solution to the intergodifferential equations is reduced to the solution of an SLAE, the matrix elements of which are expressed in the form of Fourier integrals. Such representation of kernels and matrix elements makes it possible to easily overcome the problems related to kernel peculiarities and to reduce the calculation time by about one order of magnitude. The rapid internal convergence of the solution is demonstrated. The effects of the substrate on the amplitude–frequency characteristics and the scattering pattern of a CNT antenna were investigated. It was revealed that the frequency dependence of the scattered field is resonant, with the resonances being observed by wavelengths much larger than CNT sizes. The approach of CNTs yields an increase, both in the resonance frequency and the scattered field amplitude. The dependence of the amplitude of the number of nanovibrators is nonlinear. It is shown that it is impossible to construct a directional nanosize antenna array from CNTs.

ACKNOWLEDGMENTS

The study was supported by the Russian Foundation for Basic Research, project no. 09-02-13530 ofi_tz.

APPENDIX

The calculation of the directivity pattern is based on determining the asymptotic form of a two-dimensional Fourier integral (7). Let us start from the more general problem lying in determining the integral

$$I(X) = \int_{-\infty}^{\infty}\int_{-\infty}^{\infty} q(\alpha, \beta)\exp[-p(\alpha, \beta, X)]d\alpha d\beta,$$

where $p(\alpha, \beta, X)$ depend on the parameter $X \longrightarrow \infty$.

We assume that there is a stationary point (α_0, β_0) which is determined from the equations

$$\frac{\partial p(\alpha_0, \beta_0 X)}{\partial \alpha} = 0, \quad \frac{\partial p(\alpha_0, \beta_0, X)}{\partial \beta} = 0.$$

Then

$$p(\alpha, \beta, X) \approx p(\alpha_0, \beta_0, X) + p''_{\alpha\alpha}(\alpha_0, \beta_0)(\alpha - \alpha_0)^2/2 + p''_{\beta\beta}(\alpha_0, \beta_0)(\beta - \beta_0)^2/2 + p''_{\beta\beta}(\alpha_0, \beta_0)(\alpha - \alpha_0)(\beta - \beta_0),$$

$$I(X) \sim (\alpha_0, \beta_0)\exp[-p(\alpha_0, \beta_0, X)]U(X),$$

where

$$U(X) = \int_{-\infty}^{\infty}\int_{-\infty}^{\infty}\exp\left[-p''_{\alpha\alpha}(\alpha_0, \beta_0)\frac{\alpha^2}{2} - p''_{\beta\beta}(\alpha_0, \beta_0)\frac{\beta^2}{2} - p''_{\alpha\beta}(\alpha_0, \beta_0)\alpha\beta\right]d\alpha d\beta.$$

Having performed the integration, we get

$$I(X) \approx \frac{2\pi q(\alpha_0, \beta_0)\exp[-p(\alpha_0, \beta_0)]}{\sqrt{p''_{\alpha\alpha}(\alpha_0, \beta_0)p''_{\beta\beta}(\alpha_0, \beta_0) - (p''_{\alpha\beta}(\alpha_0, \beta_0))^2}}. \quad \text{(A1)}$$

We apply (A1) to the integral

$$\frac{1}{8\pi^2}\int_{-\infty}^{\infty}\int_{-\infty}^{\infty} f(\alpha, \beta)\frac{\exp(-\gamma z)}{\gamma}\exp[-i(\alpha x + \beta y)]d\alpha d\beta \quad \text{(A2)}$$

$$\approx f(k\sin\theta\cos\varphi, k\sin\theta\sin\varphi)\exp[-ikr]\frac{1}{4\pi r}.$$

Let us use (A2) for determining the asymptotic form of integral (7). Since the coordinate of the observation point is $z > L$, then $z > z'$. Thus,

$$g(x, x', y, y', z, z') = \frac{1}{8\pi^2}\int_{-\infty}^{\infty}\int_{-\infty}^{\infty}[e^{-\gamma_1(z-z')} + Q(\rho)e^{-\gamma_1(z+z')}]\frac{1}{\gamma_1}e^{i\alpha\bar{x} + i\beta\bar{y}}d\alpha d\beta,$$

where $x' = x_c$, $y' = y_c$ are the coordinates of the vibrator center. Applying (A2), we get

$$g(x, x', y, y', z, z') \approx f(\alpha_0, \beta_0, z')\exp[-ik_1 r]\frac{1}{4\pi r},$$

where

$$f(\alpha, \beta, z') = [e^{\gamma_1 z'} + Q(\rho)e^{-\gamma_1 z'}]\exp[-i(\alpha x_c + \beta y_c)],$$

$$\alpha_0 = -k_1\sin\theta\cos\varphi, \quad \beta_0 = -k_1\sin\theta\sin\varphi,$$

$$\gamma_1 = ik_1\sin\theta, \quad \gamma_2 = \sqrt{k_2^2 - k_1^2\sin^2\theta}.$$

The vector potential in the far zone is

$$A(\varphi, \theta, r) \approx F(\varphi, \theta)\exp[-ik_1 r]\frac{1}{4\pi r}e_z$$

$$= F_a(\varphi, \theta)\exp[-ik_1 r]\frac{1}{4\pi r}(\cos\theta e_r - \sin\theta e_\theta),$$

where

$$F_a(\varphi, \theta) = \int_0^L j(z')f(\alpha_0, \beta_0, z')dz'.$$

In the far zone

$$E_\theta = Z_c\sqrt{\frac{\mu}{\varepsilon}}H_\varphi(\varphi, \theta, r)H_\varphi(\varphi, \theta, r)$$

$$\approx \frac{\partial A_\theta}{\partial r} \approx ik_1\sin\theta F_a(\varphi, \theta)\exp[-ik_1 r]\frac{1}{4\pi r},$$

where Z_c is the wave resistance in vacuum.

An analogous method for determining the field in a far zone was used in [9] as well. However, the corresponding calculations are omitted in [9].

REFERENCES

1. P. J. Burke, Li. Shengdong, and Yu. Zhen, IEEE Trans. Nanotechnol. **5**, 314 (2006).
2. G. W. Hanson, IEEE Trans. Antennas Propagat. **54**, 76 (2006).
3. G. W. Hanson, IEEE Trans. Nanotechnol. **53**, 3426 (2005).
4. J. Hao and G. W. Hanson, IEEE Trans. Nnotechnol. **5**, 766 (2006).
5. A. M. Shuba, G. Ya. Slepyan, and S. A. Maksimenko, Phys. Rev. **79**, 155403 (2009).
6. A. M. Attiya, Progress Electromagn. Res. **94**, 419 (2009).
7. G. W. Hanson, IEEE Antennas Propagat. Mag. **50** (3), 66 (2008).
8. K. Kempa, B. Kimball, J. Ryhczynski, et al., Adv. Mater. **19**, 421 (2007).
9. A. M. Lerer, Vestn. Mosk. Univ., Fiz. Astron., No. 5, 43 (2010).
10. A. B. Kleshchenkov, A. M. Lerer, and O. S. Labun'ko, Usp. Sovrem. Radioelektron., No. 6, 60 (2006).